AD NUMBER
AD596285
CLASSIFICATION CHANGES
TO: **unclassified**
FROM: **confidential**
LIMITATION CHANGES
TO: **Approved for public release; distribution is unlimited.**
FROM: **Distribution authorized to DoD and DoD contractors only; Foreign Government Information; NOV 1971. Other requests shall be referred to British Embassy, 3100 Massachusetts Avenue, NW, Washington, DC 20008.**
AUTHORITY
DSTL ltr dtd 12 Dec 2006; DSTL ltr dtd 12 Dec 2006

ROCKET PROPULSION ESTABLISHMENT
WESTCOTT

R.P.E. TECHNICAL REPORT No. 71/11

RADIO INTERFERENCE DUE TO ROCKET EXHAUST JETS: THE MEASUREMENT AND COMPUTER MODELLING OF AMPLITUDE AND PHASE NOISE SPECTRA

by

H. Williams

NOVEMBER 1971

RELEASE CONDITIONS FOR OVERSEAS DISTRIBUTION

A

1. THIS INFORMATION IS RELEASED BY THE UK GOVERNMENT TO THE RECIPIENT GOVERNMENT FOR DEFENCE PURPOSES ONLY.
2. THIS INFORMATION MUST BE ACCORDED THE SAME DEGREE OF SECURITY PROTECTION AS THAT ACCORDED THERETO BY THE UK GOVERNMENT.
3. THIS INFORMATION MAY BE DISCLOSED ONLY WITHIN THE DEFENCE DEPARTMENTS OF THE RECIPIENT GOVERNMENT AND TO ITS DEFENCE CONTRACTORS WITHIN ITS OWN TERRITORY, EXCEPT AS OTHERWISE AUTHORISED BY THE MINISTRY OF DEFENCE (PROCUREMENT EXECUTIVE) REPORTS CENTRE. SUCH RECIPIENTS SHALL BE REQUIRED TO ACCEPT THE INFORMATION ON THE SAME CONDITIONS AS THE RECIPIENT GOVERNMENT.
4. THIS INFORMATION MAY BE SUBJECT TO PRIVATELY-OWNED RIGHTS.

B

1. THIS INFORMATION IS RELEASED BY THE UK GOVERNMENT TO THE RECIPIENT GOVERNMENT FOR DEFENCE PURPOSES ONLY.
2. THIS INFORMATION MUST BE ACCORDED THE SAME DEGREE OF SECURITY PROTECTION AS THAT ACCORDED THERETO BY THE UK GOVERNMENT.
3. THIS INFORMATION MAY BE DISCLOSED ONLY WITHIN THE DEFENCE DEPARTMENTS OF THE RECIPIENT GOVERNMENT AND TO THOSE NOTED IN THE ATTACHED LIST, EXCEPT AS OTHERWISE AUTHORISED BY THE MINISTRY OF DEFENCE (PROCUREMENT EXECUTIVE) REPORTS CENTRE. SUCH RECIPIENTS SHALL BE REQUIRED TO ACCEPT THE INFORMATION ON THE SAME CONDITIONS AS THE RECIPIENT GOVERNMENT.
4. THIS INFORMATION MAY BE SUBJECT TO PRIVATELY-OWNED RIGHTS.

C

1. THIS INFORMATION IS RELEASED BY THE UK GOVERNMENT TO THE RECIPIENT GOVERNMENT FOR DEFENCE PURPOSES ONLY.
2. THIS INFORMATION MUST BE ACCORDED THE SAME DEGREE OF SECURITY PROTECTION AS THAT ACCORDED THERETO BY THE UK GOVERNMENT.
3. THIS INFORMATION MAY BE DISCLOSED ONLY WITHIN THE DEFENCE DEPARTMENTS OF THE RECIPIENT GOVERNMENT, EXCEPT AS OTHERWISE AUTHORISED BY THE MINISTRY OF DEFENCE (PROCUREMENT EXECUTIVE) REPORTS CENTRE.
4. THIS INFORMATION MAY BE SUBJECT TO PRIVATELY-OWNED RIGHTS.

D

5. THIS INFORMATION IS RELEASED FOR INFORMATION ONLY AND IS TO BE TREATED AS DISCLOSED IN CONFIDENCE. THE RECIPIENT GOVERNMENT SHALL USE ITS BEST ENDEAVOURS TO ENSURE THAT THIS INFORMATION IS NOT DEALT WITH IN ANY MANNER LIKELY TO PREJUDICE THE RIGHTS OF ANY OWNER THEREOF TO OBTAIN PATENT OR OTHER STATUTORY PROTECTION THEREFOR.
6. BEFORE ANY USE IS MADE OF THIS INFORMATION FOR THE PURPOSE OF MANUFACTURE, THE AUTHORISATION OF THE MINISTRY OF DEFENCE (PROCUREMENT EXECUTIVE) REPORTS CENTRE MUST BE OBTAINED.

UDC 621.396.82: 621.455

ROCKET PROPULSION ESTABLISHMENT, Gt. Brit.
WESTCOTT

Technical Report No. 71/11
November 1971

RADIO INTERFERENCE DUE TO ROCKET EXHAUST JETS: THE MEASUREMENT AND COMPUTER MODELLING OF AMPLITUDE AND PHASE NOISE SPECTRA

by

H. Williams

SUMMARY

A full description is given of a computer model developed to describe amplitude and phase noise spectra generated by incoherent volume scattering in the turbulent ionised exhaust jet.

The experimental method and equipment are described in detail and, by choice of a computer model for the jet velocity and density structure, a comparison is made between the measured and the computed noise power spectrum density functions. The agreement is excellent for the particular moderately ionised jet selected. Velocity turbulence is not found to be significant in establishing the noise spectrum. The radial and longitudinal gradients in the steady mean local velocity within the jet adequately predict the observed spectrum function.

Paper presented at the Sixth JANNAF Conference on Rocket Exhaust Plume Technology, Monterey, California, March 1971

CONTENTS

1 INTRODUCTION

The addition of amplitude noise to a microwave carrier by turbulent, ionised rocket exhaust jets has been studied in the UK and spectra recorded since the early nineteen sixties. A system capable of measuring both phase and amplitude noise powers was added in 1967 and sited at the RPE, Westcott. The system permits noise spectra to be recorded down to -120 db/Hz below the carrier level and out to 200 KHz off the carrier frequency.

In 1966 a simple model was proposed[1] for radio wave scattering in rocket exhaust jets and found capable of explaining much of the gross character of the amplitude noise spectra observed. Early computations[2] agreed well with experiment.

It is the purpose of this report to describe in some detail the form of the computer model now in use, to give a brief description of the microwave instrumentation, and finally to compare computed noise power spectrum functions with the experimental data.

In constructing a quantitative model of electromagnetic wave scattering by a turbulent rocket exhaust jet it is necessary to make physical and mathematical approximations and assumptions. This is because of both the complexity of the problem and the lack of knowledge in a number of important areas.

To test the scattering model a detailed knowledge of jet structure is required. Furthermore, accurate and unambiguous experimental data are only available for rocket motors tethered at ground level. As a result the jet description chosen is particular to such motors. The essential property of this model is simplicity resulting in ease of computation. There are other models available[3,4,5] of more general applicability, one of which[3] is regularly in use at the RPE, and there are certain to be other and better ones in the future. The overall method of approach has therefore been one of flexibility throughout. In particular the algebraic union of jet and electromagnetic model has been avoided. Quadrature is used to evaluate a volume integral for the received signal due to scattering over the whole jet. Thus any concept of an exhaust jet can be considered, the jet being input to the scattering program as a number of two-dimensional (axisymmetric) arrays from a preceding computer program.

2 ELEMENTS OF THE MODEL

A diagrammatic description of radio wave single scattering by a local

turbulent volume in a rocket motor exhaust jet is shown in Fig. 1. A small fraction of the total scattered energy enters the receiving antenna at a frequency Doppler shifted with respect to the incident frequency by virtue of the relative motion of the scattering element dV with respect to the antennae. When all such volumes within the jet are summed the result is a spread of energy about the direct received carrier wave frequency. The magnitude and shape of this noise spectrum is the desired end product.

Neglecting losses along the incident and scattered ray paths, but remembering that they must be included in the final calculation, we may write the scattered power density at the receiver in the form

$$\frac{P_T G_T(\alpha_1)}{4\pi r_1^2} \frac{\sigma\, dV}{4\pi r_2^2}$$

where σ is the volume scattering cross section per unit volume defined such that if the total power contained in a section of the incident wave front having an area $\sigma\, dV$ were radiated by an isotropic radiator located at the element dV, the strength of the wave reaching the receiving antenna would be the same as the actual strength produced by scattering in the volume element dV (for other symbols see Nomenclature).

The received scattered power is

$$dP_N = \frac{P_T G_T(\alpha_1)}{4\pi r_1^2} \frac{\sigma}{4\pi r_2^2} \frac{\lambda^2 G_R(\beta_1)}{4\pi} dV \quad .$$

The total noise power received is therefore

$$P_N = \frac{\lambda^2}{(4\pi)^3} P_T \int_{vol} \frac{G_T(\alpha_1) G_R(\beta_1)}{r_1^2 r_2^2} \sigma\, dV$$

where the volume of integration includes the jet.

The direct received signal power is

$$P_S = P_T \frac{G_T(\alpha_2) G_R(\beta_2)}{R^2} \frac{\lambda^2}{(4\pi)^2} \quad .$$

In the limit of a transmitter effectively at infinity

$$\frac{P_N}{P_S} = \frac{1}{4 \pi G_R (\beta_2)} \int_{vol} \frac{G_R (\beta_1)}{r_2^2} \sigma \, dV \quad . \tag{1}$$

The Doppler frequency shift of the power scattered from the element dV is

$$f_D = \frac{u}{\lambda} (\cos \alpha_1 - \cos \beta_1)$$

or, for the transmitter at infinity,

$$f_D = \frac{u}{\lambda} (\cos \beta_2 - \cos \beta_1) \quad . \tag{2}$$

This description has for simplicity been two dimensional only. It is readily extended to three dimensions for computation purposes. In fact for all the experimental data available the transmitting antenna lies in the plane defined by the receiving antenna and the jet axis.

3 THE VOLUME SCATTERING CROSS SECTION

The derivation of the differential scattering cross section for a plane wave incident on a turbulent, under-dense plasma medium is given by Tatarski[6] (Chapter 4).

In the limit of the first Born approximation and following an electromagnetic analysis he obtains

$$d\sigma = 2 \pi k^4 \sin \psi \, \phi_n(2 k \sin \frac{\gamma}{2}) \, d\Omega \, dV \quad .$$

It follows that the cross section per unit volume is

$$\sigma = 8 \pi^2 k^4 \sin^2 \psi \, \phi_n(2 k \sin \frac{\gamma}{2}) \quad . \tag{3}$$

The spectrum function ϕ_n of the refractive index fluctuations is not known with any accuracy at the moment. Salpeter and Treiman[7] in a useful paper discuss some of its general properties and characteristics, listing amongst the possibilities the spectrum function based on the Kolmogoroff theory of turbulence previously discussed in general terms by Tatarski[6], who gives

$$\phi_n\left(2k \sin\frac{\gamma}{2}\right) = \frac{\Gamma\left(\eta + \frac{3}{2}\right)}{\pi \sqrt{\pi}\, \Gamma(\eta)} \frac{n_1^2 a^3}{\left(1 + 4a^2 k^2 \sin^2\frac{\gamma}{2}\right)^{\eta + 3/2}} .$$

Putting $\eta = \frac{1}{3}$,

$$\phi_n\left(2k \sin\frac{\gamma}{2}\right) = \frac{0.062\, n_1^2 a^3}{\left(1 + 4a^2 k^2 \sin^2\frac{\gamma}{2}\right)^{11/6}} . \qquad (4)$$

To a good approximation at microwave frequencies

$$n = 1 - \frac{2\pi N e^2}{m(\omega^2 + \nu^2)} .$$

With $N = \bar{N} + N_1$ we obtain for the mean square fluctuation in refractive index

$$\overline{n_1^2} = \frac{4\pi^2 \overline{N_1^2} e^4}{m^2 (\omega^2 + \nu^2)^2} . \qquad (5)$$

Substitution gives

$$\sigma = \frac{32\pi^4 r_e^2}{\left(1 + \frac{\nu^2}{\omega^2}\right)^2} I^2 (\bar{N})^2 \frac{\sin^2\psi\, 0.062\, a^3}{\left(1 + 4a^2 k^2 \sin^2\frac{\gamma}{2}\right)^{11/6}} \text{ cm}^{-1} \qquad (6)$$

where $I = \frac{(\overline{N_1^2})^{\frac{1}{2}}}{\bar{N}}$ is the turbulent intensity.

The Born solution (equation (3)) assumes that the incident wave is everywhere unperturbed by the turbulent medium. In fact as the electron density increases both the incident and scattered wave will suffer attenuation through absorption and scattering loss. In this model an attempt is made to extend the validity of the single scatter description to attenuating media by calculation of these losses. Along both the incident and scattered ray the absorption per unit path length is taken as

$$\delta_a = - \frac{0.46\ \bar{N}\ \nu}{\omega^2 + \nu^2} \quad \text{db cm}^{-1} \quad .$$

The loss due to scattering along incident and scattered rays is

$$\delta_s = \frac{\sigma_s}{0.2303} \quad \text{db cm}^{-1}$$

where σ_s is the total scattering cross section. To obtain this the differential scattering cross section must be integrated over all solid angles. We obtain

$$\sigma_s = \frac{8\ \pi^3\ r_e^{\,2}\ I^2\ \bar{N}^2\ 0.062\ a^3}{(1 + \nu^2/\omega^2)^2}\ Q$$

where

$$Q = \frac{6\pi}{p^3} \left[- \frac{1}{5} (2p^2 + 2p + 1) \{ (1 + 2p)^{-5/6} - 1 \} - \right.$$

$$\left. - 2(1 + p) \{ (1 + 2p)^{1/6} - 1 \} + \frac{1}{7} \{ (1 + 2p)^{7/6} - 1 \} \right]$$

and $p = 2\ a^2\ k^2$.

The total attenuation per unit path length is $\delta_T = \delta_a + \delta_s$. Integration of δ_T along both incident and scattered paths to and from a volume element dV , taking account of the variation in plasma properties along the paths, gives the reduction in the received scattered power caused

by absorption and volume scattering. This may be evaluated readily if all plasma properties are known.

4 THE ROCKET JET MODEL[19]

Several models of turbulent reacting flow are already in existence[3,4,5]. A rigorous treatment of the physical and chemical processes involved in the mixing of a hot combustible gas with air has not been attempted in this work; rather the emphasis has been placed on a mainly empirical approach which allows a rapid and simple estimate of the gross features of the jet. The treatment falls naturally and conveniently into two parts; the fluid flow field of the jet is described first, followed by a description of the electron density field.

The method used to determine the nozzle exit plane condition, which constitutes the starting point of the jet model, is based on an implicit, one-dimensional approximation of nozzle flow, including finite rate chemistry.

4.1 The jet flow field

The jet consists of a mixing region of annular cross section and a core consisting only of exhaust products; the annulus increases in width approximately linearly with distance from the exit plane until at some axial distance L it extends across the whole width of the jet. The distance L is termed the core length, because it defines the axial extent of the core of undisturbed jet fluid, roughly conical in shape, based on the nozzle exit diameter. Beyond the core, where the jet gas is mixing with the atmosphere at all points within the jet, two regions have been described by experimental observers: first a transition region, over which the effect of the core and any particular flow properties are dissipated, and secondly what is termed the fully developed region, in which it is possible to find semi-empirical formulae for many of the jet properties. This region - the "far field" of the fluid flow - is usually the least interesting insofar as radio interference is concerned. However use is made of the expressions derived for this region as in rocket exhaust jets the transition region is relatively short. Because of this and the difficulty of finding an adequate description of the transition region it is assumed in the jet model that transition from the core region to the fully developed mixing region takes place over a negligibly small distance.

The conical nozzle, which has an expanding section in the form of a truncated cone, is the most widely used nozzle design. There are no conditions

under which the conical nozzle will produce a jet which is free of shocks. Even when the exit plane pressure is equal to the ambient pressure the approximately radial flow produced by the expansion cone means that the jet gas continues to expand after it has left the nozzle. A full description of the jet must take some account of the shocks formed within the flow. However, experimental evidence has been presented[8] for non-reacting jets to suggest that to a first approximation the shock structure does not affect the flow field of the jet. Hence it is assumed that the jet may be equated to the jet from a correctly expanded contoured nozzle, for which the central core has constant properties throughout its length.

A correction is applied to allow for the pressure adjustment in the jet which occurs when the motor is operated at other than its design conditions. The jet gas is allowed to expand inviscidly from the nozzle lip until the tangent to the inviscid jet boundary is parallel to the jet axis, Fig. 2. The calculation of the inviscid portion of the jet when the exit plane pressure is greater than the ambient pressure is accomplished by means of a method of characteristics computer program of general applicability[11]; when the exit plane pressure is less than that in the surrounding air the curvature of the shock and jet boundary are determined by an approximate method. This method of approximating the separating streamline is set out in the Appendix. Having established the initial portion of the jet it is assumed that mixing takes place from this point onwards.

This procedure is a convenient, if much simplified, way of allowing for the under- or over-expansion. Its major effect is one of changing the scale of the jet; that part of the jet downstream of x_m (Fig. 2) behaves as if it were produced by a parallel-flow nozzle of radius r_m. The core and mixing layer are accordingly non-dimensionalized by the radius r_m. This approach to the problem of incorrect expansion is similar to that suggested by Donaldson and Gray[8]. It is acknowledged that this simple treatment will not adequately describe the mixing region over the first portion of the jet; indeed comparisons of calculated and experimental attenuation levels close to the jet exit plane have indicated, as might be expected, that some allowance for mixing must be made in this section of the flow. However, the success of this correction in describing the overall scale and general behaviour of the rest of the jet is such that no major modification is envisaged at the time of writing.

The model is made quantitative by the introduction of several empirical

relationships. The core length L is assumed to be a function of the Mach number M_m on the axis at x_m, and is given by

$$\frac{L}{r_m} = 2.1\, M_m^{\,2} \quad . \tag{7}$$

This simple relationship provides a reliable estimate of the longitudinal scale of the jet, and has been tested for several practical cases under widely different exit plane conditions. Typical results are tabulated below:

	p_j/p_m	L/r_m equation (7)	L, calculated, metres	L, observed, metres
Rocket 1	0.07	21.5	0.23	0.22
Rocket 2	0.5	25.4	2.1	1.9
Rocket 3	2.0	32.5	3.7	4.0

The core is assumed to be a cone, centred on the jet axis, of base radius r_m and height L, so that the generator is given by

$$\frac{r_i}{r_m} = 1 - \frac{X}{L} \quad . \tag{8}$$

The gas velocity is assumed to remain constant throughout the core, and is allowed to decay on the axis beyond the core inversely with x, such that

$$\frac{u_b}{u_{core}} = \frac{L}{x} \quad . \tag{9}$$

The rate of decay of velocity on the jet axis has been the subject of experimental studies (see, for example, ref. 9) in which the observed rate has been measured variously between x^{-1} and x^{-2}. Measurements made at the RPE in cold non-reacting jets have indicated x^{-1} and this dependence is used in the model in the absence of any demonstrably better relationship[10].

The radial variation of the longitudinal velocity component in the mixing

region is expressed as an exponential function of position

$$\frac{u}{u_i} = \exp\left[-\ln(2)\left(\frac{r - r_i}{r_{\frac{1}{2}} - r_i}\right)^2\right] \qquad (10)$$

where $u_i = u_{core}$ if $x \leq L$;

$u_i = u$ if $x > L$;

$r_i = 0$ if $x > L$;

$r_{\frac{1}{2}}$ is the radial co-ordinate at which $u = u_i/2$.

This expression is similar to that used by Donaldson and Gray[8] but has been modified to give a continuous value of $\delta u/\delta r$ at $r = r_i$. The use of the same function for both the annular mixing region and the fully developed mixing region implies that the whole of the turbulent mixing layer is self-preserving. Although self-preservation of the velocity profile is a property of the fully developed region it is not strictly applicable to the rest of the mixing region. However measurements of velocity profiles in a rocket jet have established that the use of equation (10) gives sufficiently good agreement with experimental results.

To establish an expression for $r_{\frac{1}{2}}$ it is necessary to consider the longitudinal momentum in the jet. The integral of the rate of flow of momentum across a plane perpendicular to the axis is a constant of the system

$$\int_0^\infty \rho\, u^2\, 2\pi r\, dr = \text{constant} = \rho_j\, u_j^2\, \pi r_j^2 \qquad (11)$$

in which ρ_j is the exit plane density

u_j is the exit plane velocity

r_j is the exit plane radius .

As u is a known integrable function of r (equation (10)) it is only necessary to define ρ as a function of r to be able to deduce $r_{\frac{1}{2}}$ as a function of position. In a cold non-reacting jet it is possible to invoke the similarity relationship.

$$\frac{\rho - \rho_a}{\rho_i - \rho_a} = \left(\frac{u}{u_i} \right)^{Sc_t} \qquad (12)$$

where Sc_t is the turbulent Schmidt number and subscript a refers to ambient conditions. For a hot combusting rocket exhaust jet where temperatures are very much higher than the ambient temperature over most of the jet it is sufficient to assume the approximation

$$\rho(r) = \text{constant} = \rho_{core} \quad . \qquad (13)$$

The error introduced into the momentum integral by this approximation may be neglected, as at the edge of the jet, when

$$\rho \approx \rho_a > \rho_{core} \quad ,$$

the velocity has fallen to a small fraction of u_i and the contribution to the integral in this part of the jet is small.

From equations (6) and (13), with the further assumption that $\rho_{core} = \rho_j$,

$$\int_0^\infty u^2 \, r \, dr = \frac{1}{2} u_j^2 \, r_j^2 \quad ,$$

$$\int_0^{r_i} u^2 \, r \, dr + \int_{r_i}^\infty u^2 \, r \, dr = \frac{1}{2} u_j^2 \, r_j^2 \quad . \qquad (14)$$

But for $0 \leq r < r_i$ we have $u = u_{core} \equiv u_j$ so that equation (14) becomes

$$\int_{r_i}^\infty u^2 \, r \, dr = \frac{u_j^2}{2} (r_j^2 + r_i^2) \quad . \qquad (15)$$

Substitution for u from equation (10) gives

$$\int_{r_i}^{\infty} u_j^2 \exp\left[-2\ln(2)\left(\frac{r - r_i}{r_{\frac{1}{2}} - r_i}\right)^2\right] r\,dr = \frac{u_j^2}{2}(r_j^2 + r_i^2) \quad . \quad (16)$$

Writing $\bar{r} = r - r_i$, $d\bar{r} = dr$, the integral is transformed to

$$\int_0^{\infty} u_j^2 (\bar{r} + r_i) \exp\left[-z^2 \bar{r}^2\right] d\bar{r} = \frac{u_j^2}{2}(r_j^2 + r_i^2)$$

where

$$z^2 = \frac{2\ln(2)}{(r_{\frac{1}{2}} - r_i)^2} \quad , \quad (17)$$

so that

$$u_i^2 r_i \frac{\sqrt{\pi}}{2z} + \frac{u_i^2}{2z^2} = \frac{u_j^2}{2}(r_j^2 + r_i^2) \quad . \quad (18)$$

Equation (18) is a quadratic in $r_{\frac{1}{2}}$. If $x \leq L$ then $u_i = u_j$ and $r_{\frac{1}{2}}$ can be found in terms of r , which is a function of x as given by equation (8). If $x > L$ then $r_i = 0$ and $u_i = u_j\, L/x$ so that $r_{\frac{1}{2}}$ can be found directly as a function of x .

This defines the complete flow field.

4.2 The electron density field

A proper determination of the electron density distribution throughout the jet requires a knowledge of the gas temperature and composition and, if the full rigour of finite rate chemistry is to be applied, of the chemical reaction rates and of a detailed history of each part of the flow field. The complexity which an exact solution would produce is undesirable within the terms of reference of this exercise. A compromise has been reached therefore between the limits of frozen and equilibrium chemistry, at least so far as the electron density distribution is concerned.

If the chemistry of the jet, downstream of the nozzle exit plane, is assumed to be frozen (i.e. vanishing reaction rates) there can be no recombination, no secondary combustion, no heat release: the jet must behave in all respects like a single jet of heated inert gas. Under this condition the fraction f of initial jet gas per unit mass of gas in the mixing region is described by observed empirical relationships. The decay of jet gas concentration on the jet axis beyond the end of the core has been found to vary as x^{-2} (ref. 9) and the radial profile of concentration is governed by the similarity relationship

$$\frac{f}{f_i} = \left(\frac{u}{u_i} \right)^{Sc_t} . \qquad (19)$$

As in equation (10), the subscript refers to core values if $x \leqslant L$ and centre-line values if $x > L$. The first step in determining the electron density distribution in the model is to assume that the mixing region geometry is defined by the velocity flow field described in the previous section and that the (pre-combustion) composition of the gas mixture is described by the variation of f with position. Here Sc_t is assumed to be unity, as there is no better estimate appropriate to combusting systems. This drastic simplification of the mixing process is tantamount to assuming instantaneous mixing of the jet gas within the confines of the velocity field. The value of f at any point is given by

$$\left.\begin{aligned} f &= 1 \quad \text{inside the core} \quad , \\ f &= f_i \exp\left[- \ln(2) \left(\frac{r - r_i}{r_{\frac{1}{2}} - r_i} \right)^2 \right] \quad ; \\ f_i &= 1 \ , \ x \leqslant L \ ; \quad f_i = \frac{L^2}{x^2} \ , \ x > L \quad . \end{aligned}\right\} \qquad (20)$$

Having in this way specified a mixture composition at all points within the mixing region the effects of secondary combustion and heat release are simulated by allowing instantaneous reaction to equilibrium, making proper allowance for the velocity profile in the energy balance equation. The ionization reactions are assumed to be sufficiently rapid in the hottest parts of the mixing region to maintain equilibrium. Similarly in the outer edge of the jet the gas velocity is relatively low, so that the residence time of a mass of gas within the range of interest of the flow field (about two core

lengths) is fairly long; it is assumed to be sufficiently long to allow the ionic reactions to maintain equilibrium. Equilibrium electron densities are therefore assumed at the outer edge of the jet and inwards to about the centre of the mixing region. Close to the central core and, beyond the core, near the jet axis, the equilibrium electron levels are much lower than would be the case if the frozen chemistry approximation were applied. It is known that the exit plane electron density, which is used throughout the core, is well above the equilibrium concentration. Accordingly in the inner part of the mixing region the electron density follows the profile produced by turbulent diffusion from the core, i.e. equation (19). The resultant electron density profile is typically illustrated by Fig. 3. In detail the electron density at a radial point r is given by

$$\left.\begin{aligned} N &= f(r)\, N_{core} \\ \text{unless} \quad & f(r)\, N_{core} < N_{equil}(r) \\ \text{when} \quad N &= N_{equil}(r) \quad . \end{aligned}\right\} \qquad (21)$$

For the motor to be described $N_{core} = 2.10^{10}$ cm^{-3}, and the maximum N in the mixing layer is 8.10^{10} cm^{-3} .

No apologies are made for the lack of rigour in deriving this model: its justifications are its relative simplicity, ease of application and, under sea-level conditions at least, its reproduction of what are believed to be the major features of the electron density profile in a fuel-rich rocket exhaust jet, i.e. the relatively low centre-line value with a highly ionised annular region.

4.3 Collision frequency

The electron-neutral collision frequency at any point is calculated from

$$\nu = v_e \sum_i N_i\, q_i \qquad (22)$$

where

$v_e = \sqrt{\frac{8k\,T}{\pi\, m_e}}$ is the electron velocity, with usual notation;

N_i is the number density of species i ;

q_i is the electron collision cross section of species i .

In practice only a few of the species present in the exhaust gases have collision cross sections large enough to contribute to the collision frequency. These are typically H_2O , N_2 , CO and CO_2 . Thus the calculation of the equilibrium composition and temperature in the mixing region, described in the preparation of the electron density profile, serves also as the basis for determining collision frequency. ν is found to vary little throughout the jet. It has therefore been kept constant at a value of 2.10^{11} sec^{-1}.

4.4 The turbulent scale

The evaluation of the scattering cross section per unit volume requires a knowledge of the turbulent scale a (equation (6)). The particular scale of interest is that appropriate to the fluctuating electron density field in a chemically reacting turbulent flow. It has been shown both experimentally and theoretically[12] that this scale may be dependent upon the detailed rates of electron removal (recombination) in laboratory turbulent diffusion flames. In particular at a Reynolds number of $\sim 10^4$ in a flame of hydrogen/nitrogen combusting in air it has been found that transferring the dominant electron recombination process from

$$H_3O^+ + e^- \rightarrow \text{neutral products}$$

to

$$Na^+ + e^- + M \rightarrow N_a + M$$

increases the scale by a factor greater than two. According to the spectrum function ϕ_n this could make a difference of ~10 db to the power scattered at small angles.

Perhaps all that can be said at this time is that, at least toward the edge of the jet where the "local" Reynolds number is low, finite rate ionic chemistry could well play a part in determining the turbulent scale. For our purpose we shall ignore this possibility. We shall assume the electron density to be in the nature of a passive additive, frozen into the flow. This has certainly been shown to approximate to the truth by Granatstein[13] and by Garosi[14] in the high Reynolds number flow of weakly ionised argon. The latter finds a regime in the turbulent ion density power spectrum associated with the inertial subrange of Kolmogoroff in agreement with our choice for ϕ_n .

As the mixing/shear layer grows in width downstream of the motor exit, so the turbulent scale must grow in size as the turbulence develops.

In a recently published work Fisher and Johnston[15] tentatively conclude that the three-dimensional power spectrum in a Mach 3.34 cold jet approximates the -11/3 power law, but more usefully they determine the dependence of turbulent scale on shear layer width. For the angles of illumination of interest to this study we are dependent upon the radial and tangential scales defined by these authors in terms of

$$\int_{-\infty}^{\infty} \ell\,(\xi\ ,\ o)\ d\xi$$

where $\ell\,(\xi\ ,\ \tau)$ is the cross correlation coefficient between two points in the flow separated by the distance ξ and delayed by the time interval τ. As may be seen, this scale is twice the scale normally used.

From Fig. 32 of Fisher and Johnston,

$$L_y\ ,\ L_z \cong \frac{W}{3}$$

or

$$a \cong \frac{W}{6}\ .$$

To a good approximation in the jet model used, W the width of the mixing layer is given by

$$W = \frac{2\ r_m\ x}{L}$$

or

$$a = \frac{r_m\ x}{3\ L}\ . \qquad (23)$$

Thus at the end of the core $(x = L)$ the turbulent scale equals $r_m/3$ which for the motor considered here is approximately 3 cm. On the assumption that the electron density in our case and the concentration of "tracer" in that of Fisher and Johnston are both passive additives in the flow and that there are no loss mechanisms in either which have effective rates faster than that due to turbulent mixing, the identification of the two scales as equal in magnitude

is legitimate.

The expression (23) is therefore used throughout the jet to determine the local turbulent scale.

4.5 Turbulent intensity

The turbulent intensity is difficult to determine in the absence of experimental measurements of the fluctuating electron density field in the rocket jet. However there is a fair body of evidence characterised by Granatstein and Buchsbaum[16] that at high Reynolds numbers the intensity may be taken as unity. This is accepted and applied throughout the jet. The possible error introduced by such an assumption may be assessed at perhaps 6 db at the most when due account is taken of the dependence of scattering loss on this quantity and of the generally falling mean electron density with decreasing intensity at the edges of the jet. This is not considered to be too significant within the measuring accuracy of ± 3 db.

5 THE METHOD OF COMPUTATION

The method selected is entirely numerical, being based upon the division of the space comprising the jet into finite size volume elements.

The receiver is assumed to be on the "vehicle body", in the exit plane of the motor and a distance "l" from the jet axis. The jet is defined on a cylindrical co-ordinate system (x, r, θ) where x is the distance from the exit plane, r is the radius and θ is the azimuthal angle. The size of the volume element $dV = r\,dx\,dr\,d\theta$ is determined by an accuracy factor g. The number of elements of each lamina is given at any station in the jet by

$$n_r = g$$

$$n_\theta = 2g$$

$$n_x = \frac{g\,X_{max}}{R_{max}}$$

where X_{max} is the effective end of the jet, invariably taken as two cone lengths and R_{max} is the maximum radius of the jet, defined by the

$$\frac{u}{u_b} = 0.1 \text{ contour} .$$

It has been found by trial calculations that for an accuracy of ±1 db in the computed noise spectrum the total number of elements must exceed 10^6.

As the computer steps through these volume elements, considering every one in turn, it determines the velocity at the center of the element by interpolating within a two-dimensional (axisymmetric) array of local jet velocities previously calculated by a data production program based on Section 4. The condition for inclusion of an individual element is that

$$f_1 > f_D > f_2$$

where f_D is the Doppler frequecy shift and

$$f_1 = f_c + \frac{bw}{2} ,$$

$$f_2 = f_c + \frac{bw}{2} .$$

f_c is one of a predetermined number of frequency 'bins' of bandwidth bw, all required f_c and bw being entered as input.

If a particular element is to be included, then the contribution to the noise power in the frequency bin labelled 'f_c' is $W\, r\, dr\, d\theta\, dx$, less the attenuation, where W is the "weighting factor" of the element of volume $r\, dr\, d\theta\, dx$ given by

$$W = \frac{32\,\pi^4\, r_e^2}{\left(1 + \frac{\nu^2}{\omega^2}\right)^2} \frac{G_R(\beta_1)}{G_R(\beta_2)} \frac{I^2\,\bar{N}^2}{r_2^2} \frac{0.062\, a^3}{\left(1 + 4\, a^2\, k^2 \sin^2 \frac{\gamma}{2}\right)^{11/6}} .$$

It has been found convenient to enter the experimentally determined receiving antenna gain as a polynomial in terms of $\cos \beta/2$, in accordance with a least squares fit to the experimental data.

The attenuation for each element is dependent upon its position in the jet and the actual paths taken by the incident and scattered rays. Using the previously given total attenuation per unit path length ($\delta_T = \delta_a + \delta_s$) the method of calculating the total loss is to proceed in certain step lengths towards the receiver as far as the edge of the jet and then towards the transmitter as far as the edge of the jet evaluating the line integral

$$\text{Attenuation} = \int_s \delta_T(s)\, ds$$

along both paths.

The step length is itself a function of position in the jet given by

$$\frac{\bar{N}_i}{\bar{N}} \cdot \frac{L}{q}$$

where L is the length of the potential core and q is $4g$. This permits larger step lengths to be considered as the electron density, and hence loss per unit step length, decreases.

Direct attenuation, in a straight line from receiver to transmitter is also computed, see Table 1.

6 EXPERIMENTAL EQUIPMENT[20]

6.1 The amplitude and phase noise measuring system

The equipment described here was designed and manufactured by GEC (Electronics) Ltd to an agreed specification as a result of a feasibility study conducted by this same company.

The basic system consists of an X-band microwave bridge in which one arm is an air path subjected to modulation by rocket exhausts and the second arm is a coaxial cable link providing an unmodulated reference.

The transmission path lies between two aerials 31 m apart and mounted on top of towers 9 m high. A cabin is situated half-way up each tower, one containing the transmitter and the other the input stages of the receiver. The electronic equipment in each tower is protected by a specially constructed enclosure from any excessive acoustic vibration that may occur.

A control room placed 90 m from the towers houses the Main Assembly. This equipment processes the signals from the receiver, extracts the amplitude and phase modulation components and converts them into a form suitable for recording on tape. Interconnections between the three Assemblies enable the complete system to be controlled from the Main Assembly. A block diagram of the system is shown in Fig. 4.

The transmitter is a klystron operating at X-band and supplying an output power of 1.4 watts into a "hoghorn" aerial. An additional low power output feeds the reference path which is a coaxial link between the transmitter and receiver assemblies.

The receiving aerial is adjacent to the rocket exhaust and the microwave signal is passed to a mixer where it is mixed with the local oscillator signal to produce an intermediate frequency of 20 MHz. A second mixer processes the reference signal in a similar manner. The two IF signals are then amplified and coupled back to the Main Assembly through coaxial links.

Further amplification takes place before diode detection is used to separate the amplitude modulation from the carrier. The IF signals are also compared in a phase sensitive detector to obtain the phase modulation levels. The attenuation produced by the rocket efflux is measured by extracting part of the input to the signal channel IF amplifier and feeding it to a separate amplifier with manual gain control.

Following each modulation detector are three high pass filters and associated amplifiers enabling the overall modulation spectrum to be divided into discrete frequency bands suitable for recording on tape.

To check that physical movement of the receiver aerial does not introduce spurious sidebands, three transducers are mounted on the aerial, one in each plane.

Performance

Attenuation

Dynamic range	-40 db

System Resolution Amplitude and phase modulation

0 db RF attenuation	-100 db to -120 db
30 db RF attenuation	-99 db to -103 db

Cross Talk

Signal AM to PM	-27 db
PM to Signal AM	-30 db
Ref AM to PM	-10 db

6.2 Calibration

Overall calibration of the system is performed by extracting a small, precisely known amount of the transmitter output signal, modulating it 100% in amplitude with a square wave and returning it to the main path prior to transmission. Both amplitude and phase modulation may be obtained in this way by returning the modulated signal either in phase or quadrature with the carrier. The small sample of transmitter power is coupled into the auxiliary

calibration circuit from a 20 db cross coupler, via a set level attenuator, into a 3 db sidewall coupler. This coupler divides the available power equally between two identical branches wherein it is subjected to 100% modulation by means of diode modulators and recombined in a second 3 db sidewall coupler. The modulated wave is then reintroduced into the main waveguide run via another 20 db cross coupler and adjusted, by means of a phase shifter in each branch, to be either in phase for amplitude modulation or quadrature for phase modulation. Ideally, this system requires that the modulator should produce side bands only, which requires a balanced modulator and careful setting up. However, where the sideband is low, the level of the reintroduced carrier is also low and is negligible in comparison with the carrier provided by the unattenuated transmitter output. An effect is only apparent in the case of phase modulation, where it produces an amplitude modulated component, in this case more than 40 db down on the phase modulation calibration.

6.3 Receiver aerials

Of particular significance to the measurement of small levels of phase noise is the mounting of the antenna in the vicinity of the rocket jet, in this case the receiving antenna. The magnitude of the problem is illustrated by the fact that on an X-band carrier a phase modulation of $-130\ db_i$ is produced by a physical movement of the antenna by one microinch. As a consequence, following a study of the hostile environment, a receiving aerial was designed supported by six rubber shock mounts in a steel housing. This is shown mounted alongside the motor in Fig. 5.

The feed from the aerial consists of a short length of coaxitube to provide a flexible non-phase shifting connection.

Vibration transducers are used during all firings to determine the motion of the receiving aerial in three dimensions. Interpretation of these data allows a full measurement of that part of the phase noise spectrum, if any, which is attributable to acoustical vibration. In the results reported here this contribution proved to be negligible at all frequencies.

6.4 Recording and analysis

Data concentrated in the Main Assembly are brought to a 14-channel Ampex FR 1300 tape recorder. The information recorded is listed in Table 2. It will be noted that channel capacity is divided between flame interference data and a check on system performance. Both direct recording (DR) and

frequency modulated (FM) modules are employed giving a frequency recording capability from direct voltage to 300 kHz at a tape speed of 60 inches per second. The specified response "flatness" is to within ± 3 db; this is easy to obtain and can be improved with careful adjustment during alignment. A dynamic range of between 25 db and 32 db is available on DR channels depending upon tape speed, whilst that for FM channels is between 40 db and 44 db, again dependent upon tape speed, the total harmonic distortion not exceeding 2.0%.

Attenuation levels may also be displayed on a pen recorder simultaneously with recording on tape, thus permitting instantaneous information regarding this variable to be obtained.

Analysis is performed using the James Scott Spectrum Analyser Type 190 GHLA and the Brüel and Kjaer Level Recorder Type 2305. A block diagram is shown in Fig. 6.

The spectrum analyser makes a Fourier analysis of the noise power available from the amplitude and phase modulation channels of the tape recorder. Controlled manually, the levels of noise input at any frequency between 100 Hz and 200 kHz can be obtained, measured in a pre-selected bandwidth. Available bandwidths are 30 Hz, 70 Hz, 100 Hz, 500 Hz and 1000 Hz (Broadband). It will be noticed that two attachments form part of the spectrum analyser, a Low Frequency Attachment (LFA) and a High Frequency Attachment (HFA). These serve to extend the frequency coverage of the main unit which is limited to frequency operation in the range 1.0 kHz to 145 kHz. The LFA extends the lower frequency range to 100 Hz whilst the HFA increases the upper range to 200 kHz. The intrinsic noise of the analyser becomes apparent at -120 db with respect to 1.0 volt when measured in a 100 Hz bandwidth, and an accuracy of ± 3 db is achieved throughout its frequency range.

For analysis presentation a Brüel and Kjaer level recorder is used. This instrument accepts signals in the frequency range 2 Hz to 200 kHz when driven in the AC mode (three options: rms, average or peak). When direct voltage is applied it is converted to a square wave by an electromechanical "chopper" operating at 100 Hz. The subsequent process is then identical to that for alternating voltages. The dynamic range of the recorder is determined by interchangeable range potentiometers having logarithmic or linear characteristics.

7 THE ROCKET MOTOR

The motor used during these trials was the ABL EM-71 motor containing

40 lb of ELP propellent. It is well described in ref. 17. (Note that the EM-71 is a heavyweight version of the EM-27. They only differ in chamber wall thickness and end plate design.) Suffice to say here that the propellent was composite-modified double-base of the following composition:

Ingredient	Per cent, by weight
Nitrocellulose (12.6% N)	28.0
Nitroglycerin	38.3
Ammonium perchlorate	19.6
Mg (30)/Al (70) alloy	4.9
Triacetin	7.2
Resorcinol	1.0
2-nitrodiphenylamine	1.0
Alkali metal content	**ppm**
Sodium	46.5
Potassium	10
Caesium	5

The propellent burned at a calculated temperature of about 3200°K and at a chamber pressure of 260 psi, the combustion products being expanded through a nozzle of expansion ratio 5.4. The nozzle exit plane diameter was 6 inches. The fuel index of the exhaust gases was approximately 0.4, and the exit gas temperature approximately 1700°K. A thrust of 2500 lb was developed for a duration just less than 4 seconds.

8 RESULTS AND DISCUSSION

The table gives a succinct comparison between measured insertion loss and computed attenuation of the direct ray versus angle of look α . The experimental data have been averaged over the firing period and over a number of firings, and have a spread at any angle of at least ± 1 db.

Comparison of computed and experimental insertion loss

Angle of look, α	Insertion loss, db	
	Measured	Computed
+5°	5	7.6
+9°	6.5	6.5
+30°	2	1.2

The agreement is good. This is taken as adequate verification of the jet model described here. As shown elsewhere[18] the dependence of the longitudinal insertion loss on angle of look is a searching test of the adequacy of any description of the ionised jet in the absence of diffraction.

Fig. 7 and 8 show the experimental amplitude and phase noise power spectra, the bar indicating the likely error. The vertical scale is in terms of db below the incident carrier per unit bandwidth, the incident carrier being defined as the received signal level in the absence of the exhaust jet. The levelling off of the spectra at $\sim$ -120 db at the highest frequencies is due to overal system noise - particularly the magnetic-tape noise.

The first thing to notice is that amplitude and phase noise spectra are identical under all the experimental conditions. This is a first requirement for the scattering model to be correct. It may readily be shown that the incoherent summation of the scattered power from each correlated volume in the jet produces identical amplitude and phase noise spectra when quoted in db below incident carrier. The condition is that the received scattered power is much less than the received carrier power. The agreement between computed and measured spectra is excellent. Particularly noteworthy is the internal consistency in the results. At large angles of look ($\pm 30^{\circ}$) the low frequency saturation is well reproduced by the computed data. The approximate 10 db difference between the low frequency levels at $+30^{\circ}$ and -30° is well reproduced. In fact the computer output follows the changes in shape and in magnitude of the measured noise spectra over the full range of the experimental data. However the originally computed spectra are below those measured at all angles, particularly at the large ones. The very nature of the scattering cross section is such that most power is scattered about the forward direction; scattering at large angles is weak. At small angles the scattering cross section varies as the cube of the turbulent scale. One is therefore tempted to increase the scales beyond those derived from the work of Fisher and Johnston. The effect of multiplying by a factor of four is shown as the broken line in Fig. 7 and 8. The agreement between experiment and model at positive angles is improved in this way but, as one might expect, at large negative angles the opposite is true. The reason is simple in that at these negative angles the angle of scatter into the receiver is necessarily large and at large angles of scatter the scattered power varies as $a^{-2/3}$. Numerical trials have shown that the relationship chosen to describe the turbulent scale gives the best possible fit to the experimental data.

It is now with confidence that one may perform a parametric study covering the many other variables in the model. Although such a study has been completed, a full discussion here would extend this paper unduly. A separate report is intended.

Finally, it is only fair to comment that success has been achieved in the endeavour to descibe numerically the amplitude and phase noise, with the simplest of scattering models, the validity of which may be questioned on certain counts. For example no account has been taken of the velocity turbulence. In principle the random nature of the magnitude and direction of the velocity vector must spread the frequency content of the scattered signal. In this model the frequency spread in the noise spectrum stems solely from gradients in the steady mean velocity flow field. An elemental volume dV , of linear dimension less than the scale of this gradient, scatters a monochromatic signal into the receiving antenna. With the inclusion of velocity turbulence this signal must be spread across the spectrum.

A further paper will describe a Monte Carlo simulation of the scattering problem. In this simulation all events are described in terms of probability distributions. Far ranging flexibility is attained at the expense of computing time. In particular one has the option of adding a random component to the mean velocity vector, described in terms of a normal distribution with zero mean and with standard deviation as input. The result of including an isotropic velocity turbulence of standard deviation (intensity) 0.4 is shown in Fig. 9 for the case $\alpha = -30^{\circ}$. Runs were completed at $\alpha = \pm 5^{\circ}$ and $+30^{\circ}$ but in these no significant effect of velocity turbulence can be discerned.

As plotted in Fig. 9 velocity turbulence apparently lifts the power spectrum at the highest frequencies. (Not shown is the fact that this also happens at the lowest frequencies (< 100 Hz).) At first sight an improved agreement with the experimental result might be argued. However this may well be fortuitous in that at these highest frequencies we are approaching the overall system noise. Certainly the "too high" experimental results above 20 kHz at $\alpha = +30^{\circ}$ are not approached by the computed results including velocity turbulence.

The broad conclusion must be that velocity turbulence does appear to have an effect on the spectrum at the largest angles of look. However, except for -30°, the effect is within the accuracy of measurement.

Acknowledgements

There is much in this report which derives from the work of others in the Flame Physics Section RPE. In particular the author is indebted to C.C. Blake (City University, London) for the original programming of the problem and to A.S. Wilson for his untiring effort in computing work and his major contributions to Section 4, and to R.E. Lawrence for running and maintaining the experimental equipment. Miss J. Price and M. Watkins also deserve thanks for carrying through the computations. In particular the author is indebted to Dr. G.A.McD. Cummings for many helpful and stimulating discussions, and to W.T. Lord for the analysis given in the Appendix.

APPENDIX

Calculation of shock and separating streamline when $p_j < p_a$

The following equations determine the radius of curvature R_s of the shock and r'_s of the separating streamline by means of a first order expansion about the separation point:

$$r_s = M_{1s}^{-1} \left| \frac{2}{(\gamma + 1)} \left\{ 1 + \frac{(\gamma - 1)}{2} M_{1s}^2 \right\} \right|^{\frac{\gamma + 1}{4(\gamma - 1)}} \frac{t}{\alpha} \quad , \tag{1}$$

$$R_s = x\, r_s \quad , \tag{2}$$

$$r'_s = \frac{R_s}{y} \quad , \tag{3}$$

where

$$x = \frac{b_o c_2 + b_2 c_o}{b_2 c_1 - b_1 c_2}$$

$$y = \frac{b_o c_1 + b_1 c_o}{b_2 c_1 - b_1 c_2}$$

$$b_o = \sin \delta_s \cos \delta_s \left(- A + B + c \right) \cot \delta_s$$

$$b_1 = \{ 1 - \sin \delta_s \cos \delta_s \left(-A + BD + cE \right) \cot \sigma_s \} \sin \sigma_s$$

$$b_2 = \cos \left(\sigma_s - \delta_s \right)$$

$$c_o = F \cot \sigma_s$$

$$c_1 = (G + FD) \cos \sigma_s$$

$$c_2 = H \sin (\sigma_s - \delta_s)$$

$$A = \sec^2 \sigma_s$$

$$B = \frac{2 M_{1s}^2 \sin^2 \sigma_s}{(M_{1s}^2 \sin^2 \sigma_s - 1)}$$

$$C = \frac{2 M_{1s}^2 \sin^2 \sigma_s}{\left(1 + \frac{(\gamma + 1)}{2} M_{1s}^2 - M_{1s}^2 \sin^2 \sigma_2\right)}$$

$$D = 1 - \frac{\left(1 + \frac{(\gamma - 1)}{2} M_{1s}^2\right)}{(M_{1s}^2 - 1)}$$

$$E = 1 + \frac{\left(1 + \frac{(\gamma - 1)}{2} M_{1s}^2\right)}{(M_{1s}^2 - 1)} \left(\frac{(\gamma + 1)}{2} \operatorname{cosec}^2 \sigma_s - 1 \right)$$

$$F = \frac{2 \gamma M_{1s}^2 \sin^2 \sigma_s}{\left(\gamma M_{1s}^2 \sin^2 \sigma_s - \frac{\gamma - 1}{2}\right)}$$

$$G = \frac{\gamma M_{1s}^2}{(M_{1s}^2 - 1)}$$

and

$$H = \gamma M_{2s}^2 .$$

M_{1s} is the Mach number in the flow upstream of the shock, M_{2s} is the Mach number in the flow downstream of the shock. M_{2s} and δ_s are known in terms of M_{1s} and σ_s from the oblique shock relations; M_{1s} and σ_s are known in terms of the pressure ratio across the shock at separation and the ratio of the ambient pressure to the stagnation pressure ahead of the shock.

TABLE 1

Sample computer output

Microwave scattering using Kolmogoroff turbulence factor with scattering loss.

Title	-	ELP: Variable A: Slope/2; X-band	
Geometry	-	Receiver from exit plane	0.000 m
		L	0.223 m
		Alpha	0.0873 rad (5.000 deg)
		Breakpoint	1.532 m
Transmitter	-	Wavelength (Lambda)	0.0316 m
Turbulence	-	Space scale (A)	0.051 m (maximum)
		Intensity (I)	1.000
Accuracy	-	G	12
Jet	-	Length	3.830 m
		Diameter at nozzle	0.153 m
		Maximum diameter	0.331 m
Potential Core	-	Length	1.915 m
		Velocity	$2.290_{10}+03$ m/sec
		Electron density	$2.000_{10}+16$ m^{-3}
		Collision frequency	$2.000_{10}+11$ sec^{-1}

Angle of polarisation of zero with attenuation

Carrier attenuation -7.573 db

Bandwidth 30 Hz

Frequency, Hz	Noise power below carrier per unit bandwidth, db
100	-74.27
200	-75.64
500	-80.68
1000	-85.31

Bandwidth 500 Hz

Frequency, Hz	Noise power below carrier per unit bandwidth, db
1000	-85.30
2000	-91.30
5000	-100.3
10000	-108.2
20000	-118.2
50000	-140.4
100000	

Integrated power is -47.28 db below incident carrier

Apparent carrier attenuation is -7.571 db

TABLE 2

Information recorded on tape

Channel	Record Module	Information
1	FM	Longitudinal vibration (RX aerial)
2	DR	AM/low frequency
3	FM	Phase monitor
4	DR	AM/medium frequency
5	FM	Signal AGC
6	DR	AM/high frequency
7	FM	Reference AGC
8	DR	PM/low frequency
9	FM	PSD output
10	DR	PM/medium frequency
11	DR	Reference AM
12	DR	PM/high frequency
13	DR	Shuttle pulse (loop analysis purposes)
14	DR	Attenuation
15		Speech and timing (half track)

Alternative inputs available

(1) Lateral vibration

(2) Vertical vibration

Nomenclature

P_T	transmitter power
P_N	received noise power
P_S	received signal power
$G_T(\alpha)$	transmitting antenna gain
$G_R(\beta)$	receiving antenna gain
α	angle of sight at transmitter (Fig. 1)
β	angle of sight at receiver (Fig. 1)
γ	angle of scatter (Fig. 1)
r_1	distance of transmitter from element dV
r_2	distance of receiver from element dV
R	distance from receiver to transmitter
N	electron density, cm^{-3}
N_1	fluctuating part of electron density, cm^{-3}
$\bar{N}$	mean electron density, cm^{-3}
n	refractive index
n_1	fluctuating part of refractive index
$\bar{n}$	mean refractive index
f_D	Doppler frequency shift, Hz
r_e	classical electron radius = $2.8 \cdot 10^{-13}$ cm
e	electronic charge, esu
ν	electron collision frequency, sec^{-1}
k	$2\pi/\lambda$, cm^{-1}
λ	incident wavelength, cm
σ	s attering cross section/unit volume, cm^{-1}
σ_s	total scattering cross section/unit volume, cm^{-1}
I	turbulent intensity
a	turbulent scales, cm
ω	angular radio frequency
ϕ_n	spectrum function
dV	elementary volume
ψ	angle between direction of scatter and incident E vector
$d\Omega$	elementary solid angle
L	core length, cm
r_j	exit plane radius, cm
r_m	radius of jet when inviscid boundary parallel to axis, cm
x_m	distance from exit plane of point where jet radius = r_m, cm
r_i	core radius, cm

$r_{\frac{1}{2}}$ radius at which $u = u_i/2$, cm

r radial co-ordinate, cm

x axial co-ordinate, cm

M_m centre-line Mach number at x_m

u longitudinal component of velocity, cm sec^{-1}

u_i velocity at edge of core if $x \leq L$, or on the centre-line if $x > L$, cm sec^{-1}

u_b centre-line velocity, cm sec^{-1}

p_j exit plane pressure

ρ_j exit plane gas density

p_a ambient pressure

ρ_a ambient gas density

ρ gas density

ρ_{core} core gas density

Sc_t turbulent Schmidt number

ψ $r - r_i$

z $\dfrac{(2\ln(2))^{\frac{1}{2}}}{r_{\frac{1}{2}} - r_i}$

f mass fraction of original jet gas in the mixing region

f_i value of f at the edge of the core if $x \leq L$ or centre-line value of f if $x > 1$

N_{core} electron density in the core, cm^{-3}

N_{equil} equilibrium electron density, cm^{-3}

v_e electron velocity, cm sec^{-1}

W width of mixing/shear layer, cm

g accuracy parameter

θ azimuthal angle in cylindrical co-ordinate system within which the jet is defined

References

No.	Author	Title etc
1	H. Williams	A simple model of radio scattering in rocket exhaust jets RPE Tech Report 66/11 (1966)
2	H. Williams	A theoretical description of radio modulation by rocket exhaust jets RPE Tech Memo 460 (1967)
3	R.R. Mikatarian H.S. Pergament	AeroChem axisymmetric mixing with non-equilibrium chemistry computer program AeroChem TP-200, June 1969
4	A.C. Victor R.W. Buecher	An analytical approach to the turbulent mixing of co-axial jets NAVWEPS Report 9057, October 1966
5	D.B. Spalding S.V. Patankar	Heat and Mass Transfer in Boundary Layers London, Morgan-Grampian (1967)
6	V.I. Tatarski	Wave Propagation in a Turbulent Medium New York, McGraw-Hill (1961)
7	E.E. Salpeter S.B. Treiman	Backscatter of electromagnetic radiation from a turbulent plasma J. Geo. Phys. Res., 69, 5, March 1 (1964)
8	C.DuP. Donaldson K.E. Gray	Theoretical and experimental investigation of the compressible free mixing of two dissimilar gases AIAA Paper No. 65-822 (1965)
9	V. Zakkay E. Krause S.D.L. Woo	Turbulent transport properties for axisymmetric heterogeneous mixing AIAA J., 2, 139-147 (1964)

No.	Author	Title etc
10	J.A. Schetz	Analysis of the mixing and combustion of gaseous and particle-laden jets in an air stream AIAA Paper No. 69-33, AIAA 7th Aerospace Sciences Meeting, January 1969
11	A.S. Wilson	The determination of the flow fields of rocket exhaust plumes by the method of characteristics RPE Tech Memo 422 (1966)
12	R.C. Golesworthy J.M. Ridout	Ion chemistry-turbulence interaction in free-jet diffusion flames Report No. 06/70 to the TTCP D-5 RIWG Meeting, RPE Westcott, August 1970
13	V.L. Granatstein T.O. Philips	Frequency spectrum of microwaves scattered by turbulent plasma Phys. Fluids, 13, November (1970)
14	G.A. Garosi G. Bekefi M. Schultz	Response of a weakly ionised plasma to turbulent gas flow Phys. Fluids, 13, November (1970)
15	M.J. Fisher K.D. Johnston	Turbulence measurements in supersonic, shock-free jets by optical crossed-beam methods NASA Tech Note D-5206, February 1970
16	V.L. Granatstein S.J. Buchsbaum	Microwave scattering from turbulent plasma Proc. of Symp. on Turbulence of Fluids and Plasmas, New York, 1968
17	C.A. Orlich J.C. Jenks	Radar interference effects of the ELP propellant exhaust ABL TR-68/5, February 1968
18	Tripartite Technical Co-operation Program Sub Panel D-5 Radar Interference Working Group	Comparison of US and UK radar interference measurements on common solid propellent systems NWC TP 4727, December 1967

No.	Author	Title etc
19	A.S. Wilson G.A.McD. Cummings H. Williams	A simple model of a rocket exhaust jet for radio interference calculations RPE Tech Report 70/8 (1970)
20	R.E. Lawrence	Radio interference caused by rocket exhaust jets: The measurement of phase modulation RPE Tech Report 70/9 (1970)

Attached: Drgs No. RP 5367-5374
Detachable abstract cards

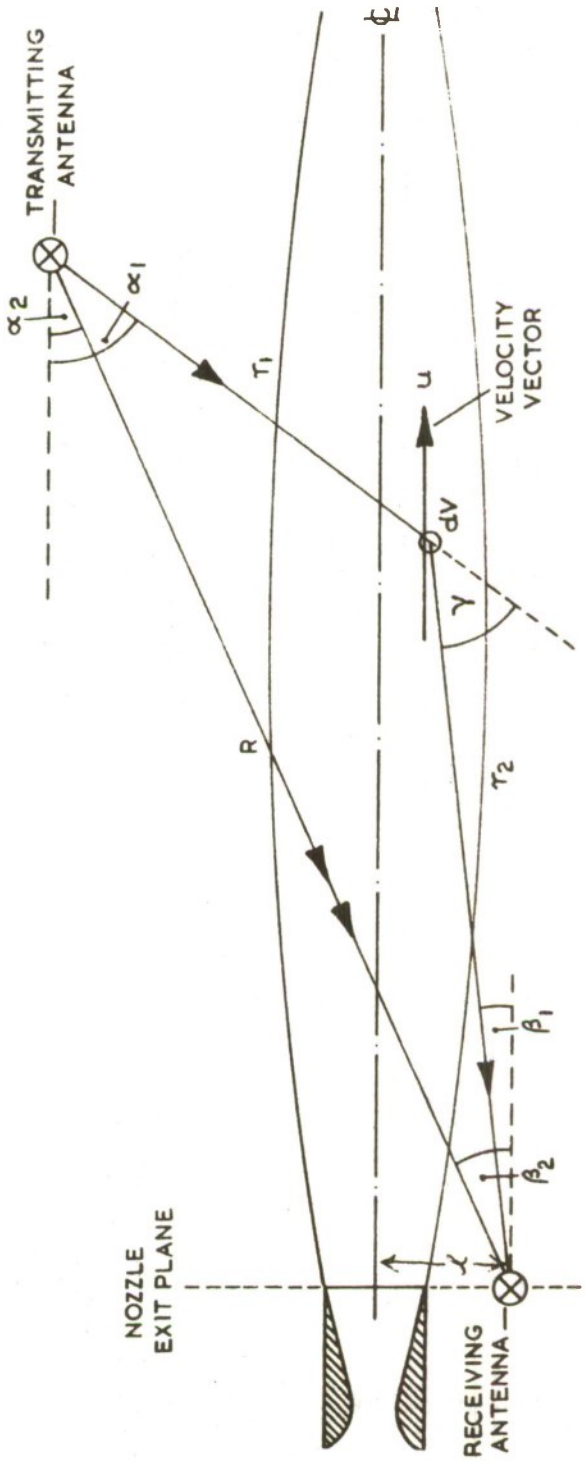

FIG. 1 GEOMETRY OF SCATTERING PROBLEMS

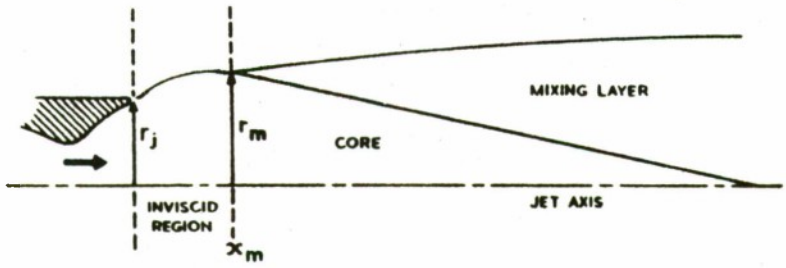

FIG. 2 METHOD OF CORRECTION WHEN NOZZLE EXIT PRESSURE IS NOT EQUAL TO AMBIENT PRESSURE

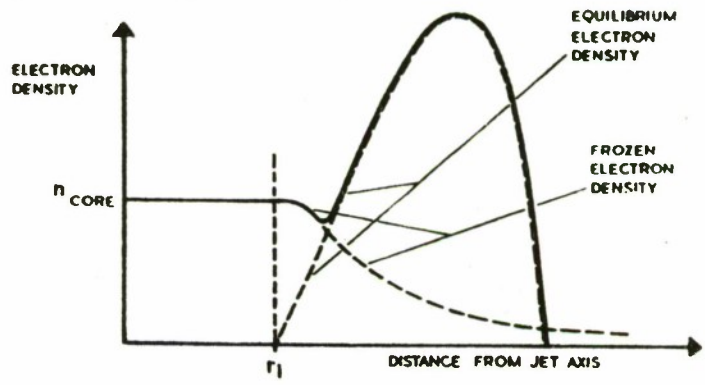

FIG. 3 DIAGRAM OF TYPICAL ELECTRON DENSITY PROFILE

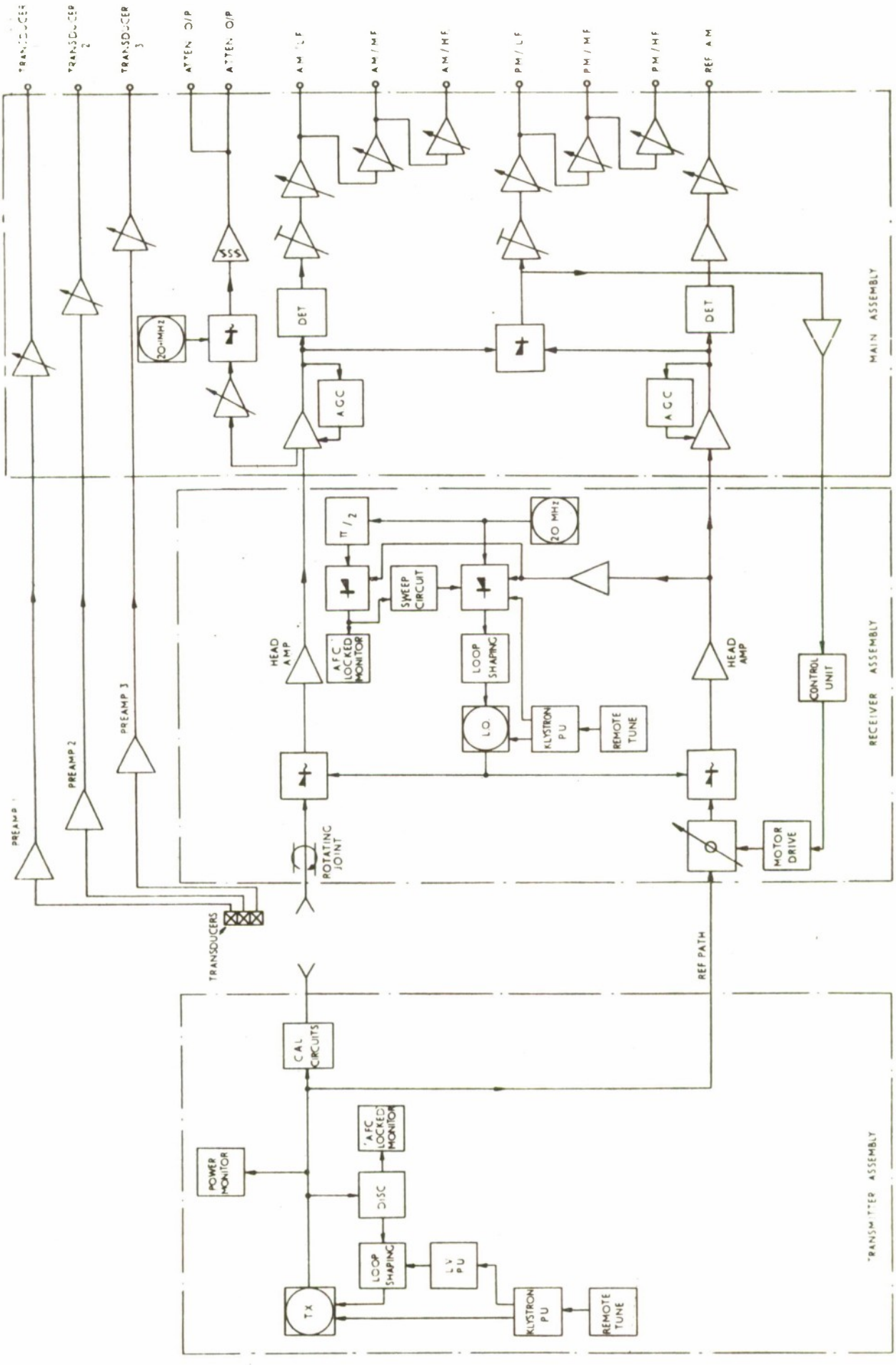

FIG. 4 BLOCK DIAGRAM OF NOISE MEASURING SYSTEM

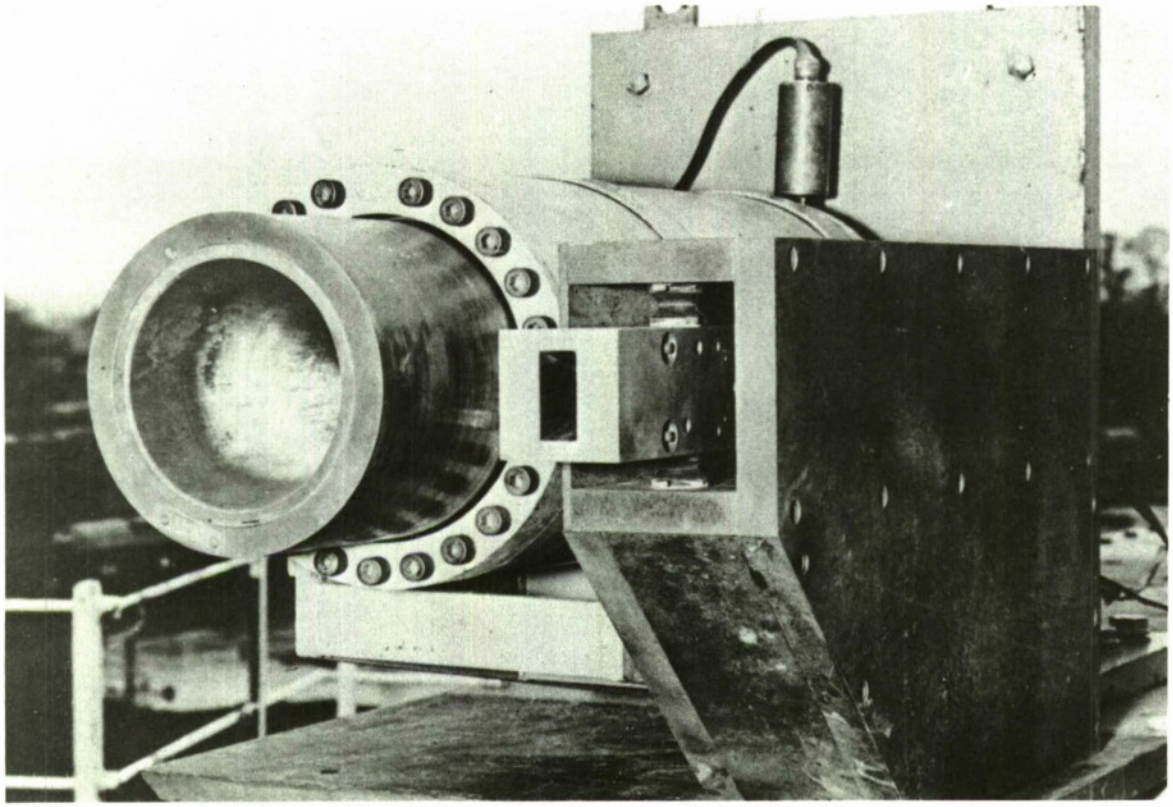

FIG. 5 RECEIVER AERIAL

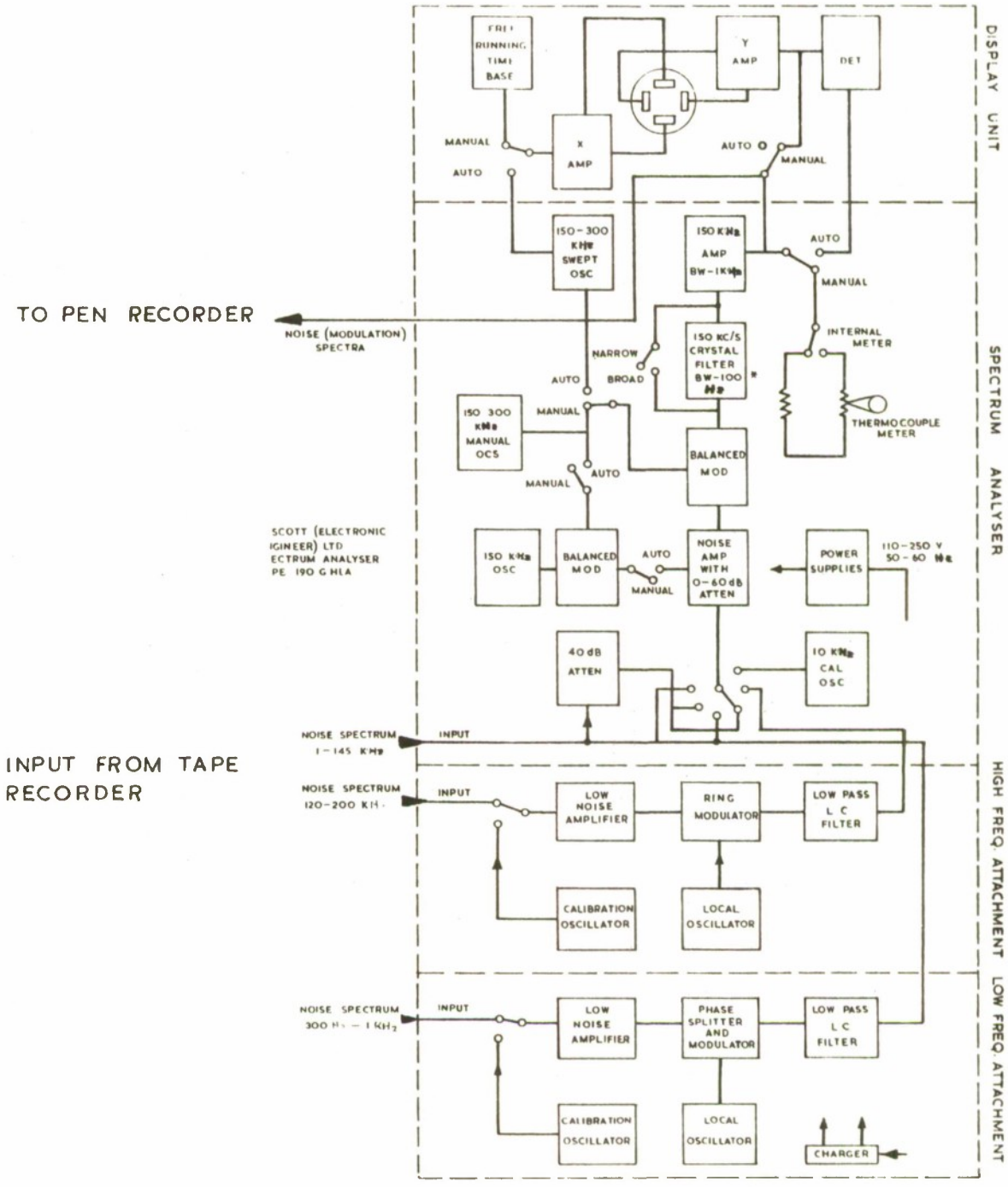

FIG. 6 BLOCK DIAGRAM OF ANALYSIS EQUIPMENT

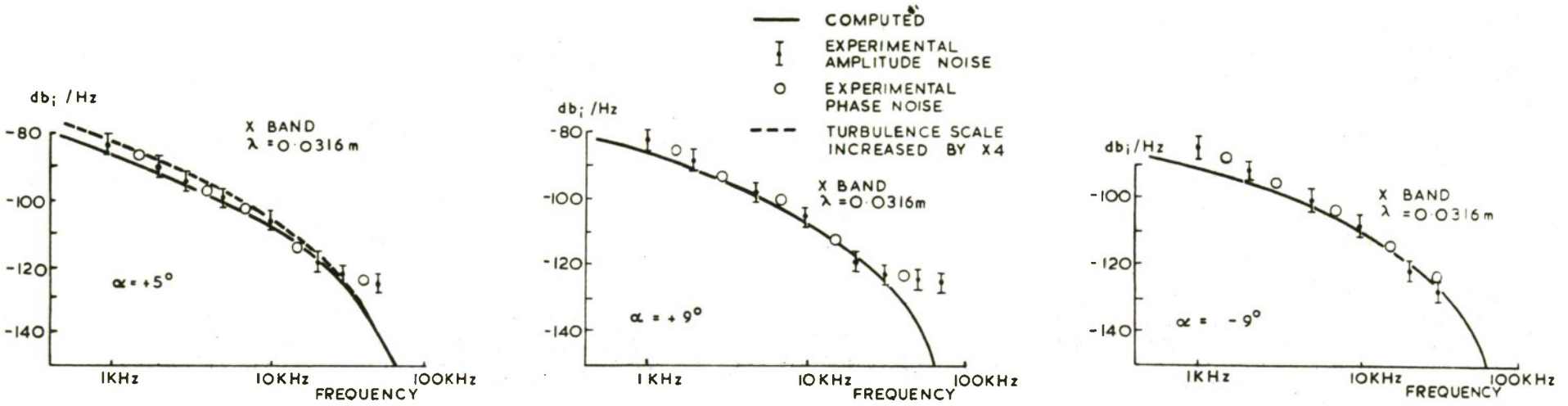

FIG.7 COMPUTED AND EXPERIMENTAL POWER SPECTRUM DENSITY FUNCTIONS $\alpha = +5°, +9°, -9°$

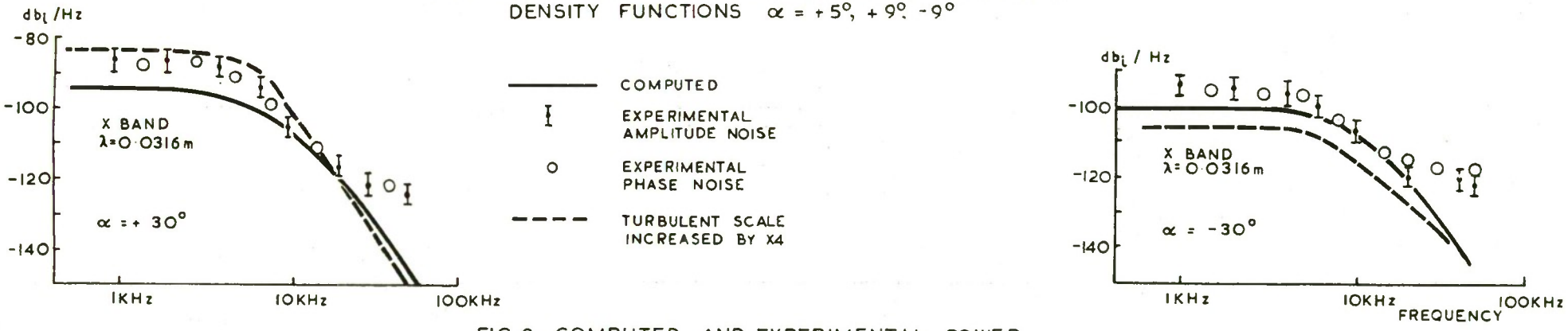

FIG.8 COMPUTED AND EXPERIMENTAL POWER SPECTRUM DENSITY FUNCTIONS. $\alpha = +30°, -30°$

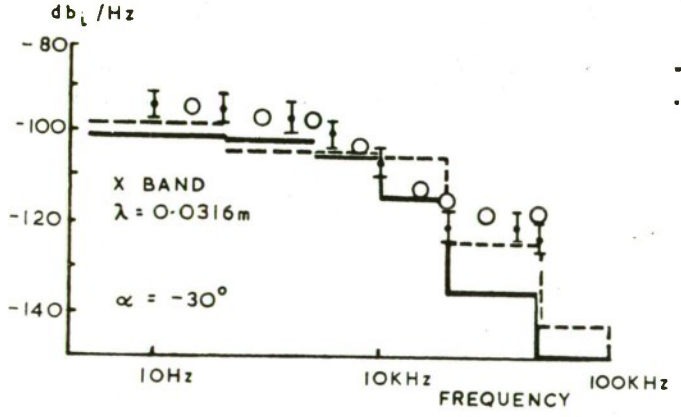

FIG. 9 COMPUTED AND EXPERIMENTAL POWER SPECTRUM DENSITY FUNCTIONS (INCLUDING VELOCITY TURBULENCE) $\alpha = -30°$

Advance distribution

MOD(PE)
Controller Establishments and Research
C/GWL
DCERB
DC/GW
DGERP(B)
DG/LRD
DGRW
D/GW(R)
D/GW(X)
D/Space
AD/GW(G&C)
AD/GW(X)
ERDE - 3
RAE Aberporth
RAE Farnborough - 6
RRE
GW(G&C)5 - 21
TRC - 200

DETACHABLE ABSTRACT CARD

CONFIDENTIAL

Williams, H. 621.396.82 : 621.455

RADIO INTERFERENCE DUE TO ROCKET EXHAUST JETS: THE MEASUREMENT AND COMPUTER MODELLING OF AMPLITUDE AND PHASE NOISE SPECTRA

Rocket Propulsion Establishment Technical Report No. 71/11 November 1971

A full description is given of a computer model developed to describe amplitude and phase noise spectra generated by incoherent volume scattering in the turbulent ionised exhaust jet.

The experimental method and equipment are described in detail and, by choice of a computer model for the jet velocity and density structure, a comparison is made between the measured and the computed noise power spectrum density functions. The agreement is excellent for the particular moderately ionised jet selected. Velocity turbulence is not found to be significant in establishing the noise spectrum. The radial and longitudinal gradients in the steady mean local velocity within the jet adequately predict the observed spectrum function.

CONFIDENTIAL

CONFIDENTIAL

Williams, H. 621.396.82 : 621.455

RADIO INTERFERENCE DUE TO ROCKET EXHAUST JETS: THE MEASUREMENT AND COMPUTER MODELLING OF AMPLITUDE AND PHASE NOISE SPECTRA

Rocket Propulsion Establishment Technical Report No. 71/11 November 1971

A full description is given of a computer model developed to describe amplitude and phase noise spectra generated by incoherent volume scattering in the turbulent ionised exhaust jet.

The experimental method and equipment are described in detail and, by choice of a computer model for the jet velocity and density structure, a comparison is made between the measured and the computed noise power spectrum density functions. The agreement is excellent for the particular moderately ionised jet selected. Velocity turbulence is not found to be significant in establishing the noise spectrum. The radial and longitudinal gradients in the steady mean local velocity within the jet adequately predict the observed spectrum function.

CONFIDENTIAL

CONFIDENTIAL

[dstl]

Information Centre
Knowledge Services
[dstl] *Porton Down*
Salisbury
Wilts
SP4 0JQ
Tel: 01980-613753
Fax 01980-613970

Defense Technical Information Center (DTIC)
8725 John J. Kingman Road, Suit 0944
Fort Belvoir, VA 22060-6218
U.S.A.

AD#: 596285
Date of Search: 12 December 2006

Record Summary:

Title: Radio interference due to rocket exhaust jets: the measurement and computer modelling of amplitude and phase noise spectra
Covering dates 1971
Availability Open Document, Open Description, Normal Closure before FOI Act: 30 years
Former reference (Department) 34327
Held by The National Archives, Kew

This document is now available at the National Archives, Kew, Surrey, United Kingdom.

DTIC has checked the National Archives Catalogue website (http://www.nationalarchives.gov.uk) and found the document is available and releasable to the public.

Access to UK public records is governed by statute, namely the Public Records Act, 1958, and the Public Records Act, 1967.
The document has been released under the 30 year rule.
(The vast majority of records selected for permanent preservation are made available to the public when they are 30 years old. This is commonly referred to as the 30 year rule and was established by the Public Records Act of 1967).

This document may be treated as UNLIMITED.


RECEIVED
25 MAR 1973
H I S A
GENERAL
MAIL ROOM